

E-RGB-D: Real-Time Event-Based Perception with Structured Light

Seyed Ehsan Marjani Bajestani and Giovanni Beltrame

Department of Computer Engineering and Software Engineering, Polytechnique
Montreal, 2500 Chem. de Polytechnique, Montreal, H3T 0A3, Quebec, Canada.

*Corresponding author(s). E-mail(s): ehsan.marjani@polymtl.ca;

Abstract

Event-based cameras (ECs) have emerged as bio-inspired sensors that report pixel brightness changes asynchronously, offering unmatched speed and efficiency in vision sensing. Despite their high dynamic range, temporal resolution, low power consumption, and computational simplicity, traditional monochrome ECs face limitations in detecting static or slowly moving objects and lack color information essential for certain applications. To address these challenges, we present a novel approach that integrates a Digital Light Processing (DLP) projector, forming Active Structured Light (ASL) for RGB-D sensing. By combining the benefits of ECs and projection-based techniques, our method enables the detection of color and the depth of each pixel separately. Dynamic projection adjustments optimize bandwidth, ensuring selective color data acquisition and yielding colorful point clouds without sacrificing spatial resolution. This integration, facilitated by a commercial TI LightCrafter 4500 projector and a monocular monochrome EC, not only enables frameless RGB-D sensing applications but also achieves remarkable performance milestones. With our approach, we achieved a color detection speed equivalent to 1400 fps and 4 kHz of pixel depth detection, significantly advancing the realm of computer vision across diverse fields from robotics to 3D reconstruction methods. Our code is publicly available: github.com/MISTLab/event_based_rgb_d_ros

Keywords: Event-based camera, Structured light, Color and Depth measurement, RGBD sensor.

1 Introduction

Event-based cameras (ECs) are innovative sensors that detect changes in pixel brightness asynchronously. Unlike traditional frame-based cameras, ECs do not capture full images, they generate events containing pixel coordinates, timestamps, and the polarity of brightness changes whenever a change exceeds a certain threshold. These sensors enable researchers to detect movement and changes at extremely high speeds with very low latency, minimal power consumption, and low

bandwidth requirements, as shown by [Marjani-Bajestani and Beltrame \(2025\)](#). It makes ECs highly suitable for high-speed vision-based applications such as depth estimation.

Depth estimation is a vital element in both computer vision and robotics, used in applications like 3D modeling, augmented reality, and navigation. Structured Light (SL) systems, which project known patterns onto a scene and observe the deformations with a camera, have traditionally been used for this purpose as described by [Geng \(2011\)](#). While accurate, these systems are limited by factors such as device bandwidth and projector

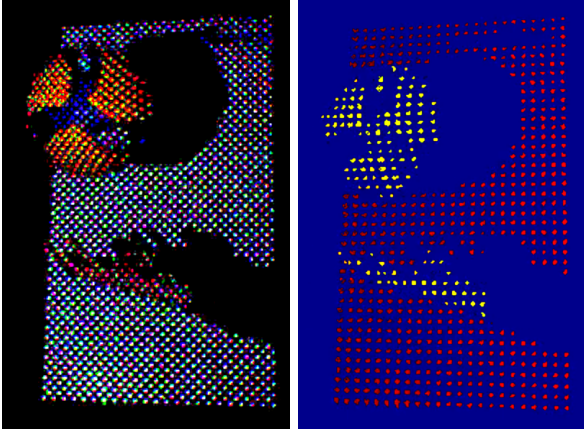


Fig. 1: Color (left) and depth (right) detection of a volleyball thrown in front of a VGA monocular event-based camera, reconstructed at 120 fps from ~ 1.5 m using the proposed method.

light power, impacting acquisition speed and performance under various lighting conditions. The high temporal resolution and high dynamic range (HDR) of ECs can address these limitations, as their asynchronous nature allows for fast, efficient data capture without the redundancy seen in frame-based systems. However, despite their advantages, traditional monochrome ECs have limitations in capturing color information.

In our previous work by [Marjani-Bajestani and Beltrame \(2023\)](#), we proposed combining an EC with a Digital Light Processing (DLP) projector to form an Active Structured Light (ASL) system for color sensing with a monochrome camera. Unlike passive color event cameras, which are currently limited in resolution and availability, our method actively generates color signals using structured projection, enabling robust reconstruction even under low-light or high-speed conditions. We extended our previous work and explained how we could achieve event-based color and depth measurements for each pixel separately. Integrating DLP projectors with ECs overcomes the constraints of traditional SL systems. The ECs' ability to suppress temporal redundancy and their high dynamic range enables effective operation in diverse lighting conditions, enhancing the depth estimation process. Additionally, the dynamic projection adjustments allow for selective color data acquisition, ensuring efficient use of bandwidth while maintaining spatial resolution. Our method

enhances depth and color detection, providing robust E-RGB-D sensing at 1.4 to 4 kHz per pixel. The main contribution is achieving ultra-fast and real-time, event-based color and depth measurements per pixel that can work in different situations within the scene.

Unlike frame-based methods such as X-maps, as proposed by [Morgenstern et al. \(2023\)](#), which require time-discretized event accumulation and rely on raster-scanned MEMS projectors, as described by [Brandli et al. \(2014\)](#), [Matsuda et al. \(2015\)](#), and [Muglikar et al. \(2021\)](#), our system operates fully asynchronously. Each event is independently tagged with depth and color without needing to reconstruct an intermediate 2D map or wait for a complete pattern sequence. This frameless design enables ultra-fast, low-latency sensing even in dynamic environments, and represents a fundamental architectural departure from prior structured light approaches. The method supports flexible structured light pattern design, enabling adaptation to various sensing conditions without modifying the core processing architecture. We validate our approach through a series of experiments that compare depth and color reconstruction performance against both event-based and traditional methods (see Section 5).

Various aspects of the main contribution are explained as follows:

High-Resolution and High-Speed 3D Reconstruction

There is always a trade-off between point cloud resolution and scanning process speed in visual-based 3D scanning systems, as discussed by [Matsuda et al. \(2015\)](#). Time-of-Flight (ToF) cameras based 3D scanners can quickly report depth information but have limitations in fast RGB detection, according to [LUCID Vision Labs \(2025\)](#). We obtained 3D reconstructions with variable resolution, allowing us to acquire a high-resolution colored 3D point cloud of an environment (in the order of millimeters, similar to 3D laser/ToF scanners but color data included), as well as high-speed 3D scanning (in the order of milliseconds with more sparse patterns).

Motion Adaptivity Across Static and Dynamic Scenes

Unlike frame-based SL systems which struggle with motion blur or fail in static scenes, our method adapts to both fast and slow motions by tuning the SL pattern and the event cameras bias settings. This makes it suitable for mobile platforms without requiring a fixed scanning speed, as shown by [Matsuda et al. \(2015\)](#). While we have not demonstrated the system on a mobile robot, this flexibility supports potential robotic integration.

Texture and Color Independence

Stereo systems are sensitive to surface texture, as noted by [Morar et al. \(2020\)](#), but our method uses active structured light and performs depth estimation independently of object texture or surface color. Additionally, by projecting light in different wavelengths, our approach improves depth reconstruction even in challenging conditions such as when the surface color closely matches the illumination wavelength or reflects little light. While color detection may degrade in such cases, depth estimation remains robust compared to traditional passive methods.

Light and Power Efficiency

Structured light approaches like Gray coding or phase-shifting, as discussed by [Gupta and Nayar \(2012\)](#), are limited by projector brightness and camera dynamic range. Our system uses a high dynamic range sensor, as proposed by [Brandli et al. \(2014\)](#), operates robustly in low-light or high-dynamic scenes, as noted by [Muglikar et al. \(2021\)](#) and [Morgenstern et al. \(2023\)](#), and minimizes power consumption by controlling the light source in response to detected events. This enables efficient 3D sensing for mobile or embedded applications, as demonstrated by [Wu et al. \(2020\)](#), [Tin et al. \(2016\)](#), and [Li et al. \(2024b\)](#).

Fast, Frame-Free Depth Computation

Our method avoids accumulating events into full frames or spatio-temporal maps, instead performing per-event depth estimation via direct stereo disparity in the projector-camera space. This design supports real-time 3D point cloud reconstruction and avoids delay-inducing computations

typical in high-speed scanning systems, as shown by [Muglikar et al. \(2021\)](#).

Scalable and Flexible Pattern Design

Our system can generate a wide range of projection patterns (e.g., coded dots, color sequences) to support specific sensing tasks. This flexibility enables adaptation to different resolution, speed, or semantic needs, and does not depend on specialized hardware. While high-speed coded patterns may require custom projection hardware, our framework is designed to accommodate these as optional extensions.

The rest of the paper is structured as follows: Section 2 discusses color detection methods; Section 3 covers event-based triangulation-based depth measurement; Section 4 describes our color and depth detection method; Section 5 details our results under various conditions; and Section 6 outlines concluding remarks and future work.

2 Monochrome to Color

Color information is essential for tasks like segmentation and recognition, as noted by [Trémeau et al. \(2008\)](#). Colorization involves creating a color image from a monochrome sensor or grayscale image without sacrificing resolution. This process relies on external data about the image’s colors obtained from external device, as described by [Jang and Jung \(2020\)](#), user input, as shown by [Levin et al. \(2004\)](#), and a trained neural network that incorporates the scene’s color information, as demonstrated by [Zhang et al. \(2016\)](#) and [Cohen Duwek and Ezra Tsur \(2024\)](#). It can be both time-consuming and costly.

The first generation of event cameras (ECs) were monochrome, with color ECs only recently becoming available, as introduced by [Li et al. \(2015\)](#), [Moeys et al. \(2017a\)](#), and [Moeys et al. \(2017b\)](#). However, color ECs have a lower resolution than monochrome ECs due to sensor size limitations and the need for color filters, as explained by [Bayer \(1976\)](#), [Khashabi et al. \(2014\)](#), and [Ramanath et al. \(2005\)](#).

To maintain resolution while tripling the bandwidth requirements, [Marcireau et al. \(2018\)](#), utilized dichroic filters on three ECs. They combined the output of three ECs, enabling the capture of color information in three distinct event streams.

In our initial work by [Marjani-Bajestani and Beltrame \(2023\)](#), we utilized a DLP projector to emit light patterns, referred to as ASL, onto a scene. The EC then captured the reflections of these patterns, generating events that were tagged with the scene’s color information. As Fig. 2 shows the proposed procedure, we are able to reconstruct full color image from a monochrome EC. Section 4 describes our method for color and depth detection in details in terms of pattern frequency and coverage. Some visible noise patterns in the reconstructed color images (e.g., Fig. 2) are due to optical interactions between the camera and projector lenses. These patterns can appear due to lens distortions or interference, particularly when using high-intensity structured projection. This factor will be addressed in future hardware refinements.

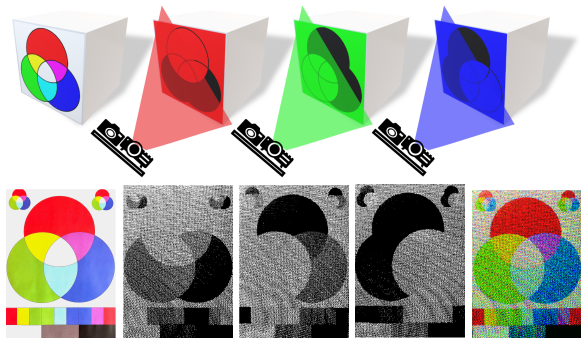


Fig. 2: Color detection of a printed color wheel, as introduced by [Marjani-Bajestani and Beltrame \(2023\)](#). Top: The proposed procedure involves projecting various light patterns in different wavelengths/colors. Bottom, from left to right: high-resolution Ground Truth (GT), reconstructed images captured by a VGA monochrome EC in the channels of Red, Green, Blue, and the fully reconstructed image.

3 Depth Sensing via Triangulation

In order to gather more information about the scene, fusion methods with an additional sensor are considered. While the interference-based methods are known as extremely accurate for micro-scale measuring, Time-of-flight methods are

well known as low-accuracy measuring methods for a large-scale scene. Triangulation-based methods would be in the middle of them, as described by [Marrugo et al. \(2020\)](#). Triangulation-based techniques, including stereo vision and SL, have been demonstrated to provide precise depth information at short distances. In this paper, we focused on event-based depth measuring via SL.

3.1 Event-based depth sensing with SL

ECs can identify SL related events due to their frequency or contrast changes. By changing the frequency of SL, the camera can detect points individually. It required to be expressed that there are two different fusions of SL and EC. The first type is when a SL device is used to *create* events and capturing those events by the camera (same as the proposed method by [Martel et al. \(2018\)](#)). The second method is to use a SL device (or any other 3D depth sensors) to obtain a depth pre-reconstruction of the scene and subsequently adding the depth information to the captured events. For instance, [Weikersdorfer et al. \(2014\)](#) used an external SL projector (Kinect) to receive the depth information of the scene. In parallel, an EC is used to obtain events (the brightness changes of each pixel due to movements), and the two outputs are merged to construct the 3D events. Therefore, despite having an active external lighting source, movement is required to generate the necessary data. Using the Kinect separately in parallel is power-consuming, and the process time would not be shortened.

In general, SL can be considered as an active stereo-vision method which uses the same concept (triangulation) for depth measurement. However, in this case, a pattern is emitted on the surface and the camera will capture the pattern deformation. Consequently, the structured pattern replaces one of the cameras in stereo-camera system. A typical SL system uses one camera and one projector; however, to reach a higher resolution or a faster full measurement, more cameras can be added as shown by [Willomitzer and Häusler \(2017\)](#) and [Zhao et al. \(2019\)](#).

The concept of using an external projector to employ SL and prevent stereo challenges with a monocular EC is foundational to modern systems employing event cameras, as shown by [Brandli](#)

Table 1: Summary of Previous SL-based Systems Addressing Depth Estimation with monocular EC

Method	EC	Sensor	Projector
Brandli et al. (2014)	DVS128	128 × 128	Laser line 500 Hz
MC3D Matsuda et al. (2015)	DVS128	128 × 128	Laser point 60 fps
FTD Leroux et al. (2018)	ATIS0	304 × 240	DLP TI LightCrafter 3000
FPP Mangalore et al. (2020); Li et al. (2024a)	DAVIS346	346 × 260	DLP TI LightCrafter 4500
ESL Muglikar et al. (2021)	Prophesee Gen3	640 × 480	Laser point 60 fps
X-maps Morgenstern et al. (2023)	Prophesee Gen3	640 × 480	Laser point 60 fps
SEG Lu et al. (2024)	Prophesee Gen4	1280 × 720	Laser point 60 fps (for static scene) DLP projector OPR305185 (for dynamic scene)
Ours E-RGB-D	Prophesee Gen3	640 × 480	DLP TI LightCrafter 4500

et al. (2014), Matsuda et al. (2015), Muglikar et al. (2021), and Morgenstern et al. (2023). Table 1 summarizes previous structured light (SL) systems that have tackled the issue of depth estimation using event cameras. The SL methods are different in terms of patterns types.

Coded patterns SL: Strips SL are introduced to perform the area scanning. If they are unique, the system can identify points and calculate the depth. If these strips are in black and white (*binary coding*), series of patterns are needed to identify the corresponding points. Thus compared to the other patterns, binary patterns are sensitive to object movement. Consequently, a high frequency of switching the binary patterns is assisting. DLP projectors have the ability to switch patterns in the order of kilohertz, as demonstrated by Wang et al. (2022) and Lu et al. (2024). To have a higher resolution, 2D and hybrid patterns are introduced by Yu et al. (2020).

Leroux et al. (2018) present a 3D reconstruction method using an Asynchronous Time-based Image Sensor (ATIS) with 304 × 240 pixels and a DLP projector. Instead of line structured light (SL), Frequency-Tagged Dots (FTD) are projected onto the scene. The known pattern and distances allow calculation of pattern deformation and point depth. This method, however, is highly sensitive to movement and ambient light changes, which affect the number of captured events.

Mangalore et al. (2020) and Li et al. (2024a) used a Dynamic Active-pixel Vision Sensor (DAVIS346, 346 × 260 pixels) with a DLP LightCrafter 4500 for 3D reconstruction. They developed a Fringe Projection Profilometry (FPP) system using a moving fringe pattern, allowing the EC to scan multiple lines simultaneously, which is faster than line-scanning methods. The EC’s

advantage is detecting shadowed areas, unlike frame-based cameras where shadows and dark regions appear the same. However, a pre-recording of the scene without the object is needed to “inpaint” shadowed areas, and the camera’s limited event reporting capacity can lead to some events being eliminated.

Simple patterns SL: The simplest method, known as the statistical pattern, involves a random distribution of dots. This method is used in various commercial devices such as Microsoft Kinect (2010), Intel RealSense (2025), and Orbbec, Astra Series (2025) due to its simplicity and small footprints. Huang et al. (2021), also frequently projected a single pseudo-random pattern using a DLP6500 projector. They generated event frames from the event stream and utilized a digital image correlation method to calculate displacements and derive 3D surfaces of target objects. While using a single dot-based pattern increased scanning speed, it sacrificed detailed information compared to dense information achievable with line-based patterns. Moreover, implementing a discrete pattern led to inaccurate dot location and sensitivity to ambient light, resulting in low-resolution 3D depth measurements, as reported by Marrugo et al. (2020).

Another way to acquire higher resolution is to use line instead of discrete dots. In that way, high accuracy measurement in one direction will be attained. This method is also combined with a line laser for short range scanning. However, to measure the depth in all directions the line direction needs to vary.

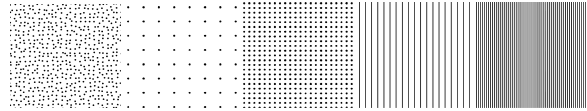
Brandli et al. (2014) used a laser line and an EC to scan the surface of an object. Using a concentrated light line (laser) helped achieve more contrast and detect the line more easily with

the EC. Additionally, if the environment is static, emitting the structured light (SL) helps detect only the relevant pixels. However, to obtain a 3D reconstruction of the scene using this method, it is necessary to change the line direction or move the object in front of the laser line.

By using the line laser and the EC, [Matsuda et al. \(2015\)](#), who introduced “Motion Contrast 3D Scanning” (MC3D), resolved the speed-resolution trade-off issue present in traditional SL scanners. Traditional SL scanners become inoperative when illumination changes occur in the environment; however, using a high dynamic range EC yields an improved final result. The laser scanner had an exposure time of 28.5 seconds, but their proposed device had an exposure time of one second.

Expanding on the Matsuda et al’s work, [Muglikar et al. \(2021\)](#), who introduced “Event-based Structured Light” (ESL), employed time maps to establish a temporal link between the projector and camera. Initially, they produced depth maps by conducting an epipolar disparity search within rectified projector time maps. Following this, an additional processing stage was implemented to enhance pixel-level coherence and reduce event fluctuations. However, this stage demands significant computational resources, preventing their method from achieving real-time performance.

[Morgenstern et al. \(2023\)](#), introduced a method that converts the projector time map into a rectified “X-map”, capturing X-axis correspondences for incoming events and enabling direct disparity lookup without additional search. This method supported real-time interactivity, making it suitable for Spatial Augmented Reality (SAR) experiences requiring low latency and high frame rates. They claimed that their method is 7 to 100 times faster than considering the entire frame, as in the ESL method, because there is no need to do a row-by-row disparity search and calculate the depth for the whole frame. We used a partially similar X-mapping method to calculate the depth for each pixel. A detailed description is provided in the next section.



Random N dots M dots N lines M lines

Fig. 3: Proposed ASL pattern types for balancing speed and detail in E-RGB-D scanning. M is greater than N , meaning more points are reconstructed and have higher Coverage Percentage (CP). We did not use a pseudo-random dot pattern to detect the depth, but it could be used to add color to methods that detect only depth, such as those proposed by [Huang et al. \(2021\)](#).

4 ASL: Adaptive Structured Light

This section introduces our adaptive structured light framework. The proposed method is to adjust the SL pattern to balance the trade-off between scanning speed and detail. Achieving a denser output requires more pixel data, but there is a limit to the number of events an EC can process simultaneously, as it may become bus-saturated. The percentage of Ground Truth (GT) points estimated by the proposed method, relative to the total number of pixels in the GT that contain data, is referred to as Fill Rate (FR), completeness, or depth map completion, as defined by [Muglikar et al. \(2021\)](#). However, to avoid reaching the camera’s bus-saturation limits, we control the number of projected points by changing pattern. We refer to the ratio of ON to OFF pixels in a pattern as the Coverage Percentage (CP), as defined by [Marjani-Bajestani and Beltrame \(2023\)](#). Each pattern type has a different CP, and each experiment is evaluated based on its FR.

The high-resolution method, which uses line-based scanning and is less sensitive to ambient light, as described by [Matsuda et al. \(2015\)](#) and [Gupta et al. \(2013\)](#), is given the highest priority among the proposed patterns, while the dot-based pattern is assigned the lowest priority. Figure 3 represents the various patterns that E-RGB-D can work with, including line-based scanning, dot-based scanning, and pseudo-random dot patterns. For instance, the SL pattern could be changed according to either the remaining battery charge or the robot’s motion speed. The robot can switch to the line method and decrease

Mode One: Color only

ID	R	G	B
250	235	235	235

Mode Two: Depth only

ID	D_1	...	D_n
260	235	...	235

Mode Three: Depth then Color

ID	D_1	...	D_n	R	G	B
270	235	...	235	235	235	235

Mode Four: Depth and Color

ID	D_1	...	D_n	D_1	...	D_n	D_1	...	D_n
280	235	...	235	235	...	235	235	...	235

Fig. 4: Pattern sequence and their exposure times in microseconds. In our experiments, we used mode 3 with two different values for n (23 and 45), and mode 4 with $n=23$. One ID for each pattern type would be enough, but we could have different IDs for each color or depth pattern mode. While this increases the total scanning time, it makes the system more robust and trackable.

the LED current (decrease the power of the projector) when the energy level reaches its critical state. This flexibility is a key advantage of our approach. The system is not tied to any fixed pattern encoding scheme; rather, it can dynamically switch between different structured light patterns depending on environmental conditions (e.g., lighting, motion), application needs (e.g., speed vs. resolution), or system constraints (e.g., power consumption). These patterns are supported by the high-speed binary projection capabilities of the DLP LightCrafter 4500, and are fully compatible with our per-event processing pipeline. This modular design makes our framework broadly applicable and adaptable to various scanning contexts without requiring any structural changes to the method.

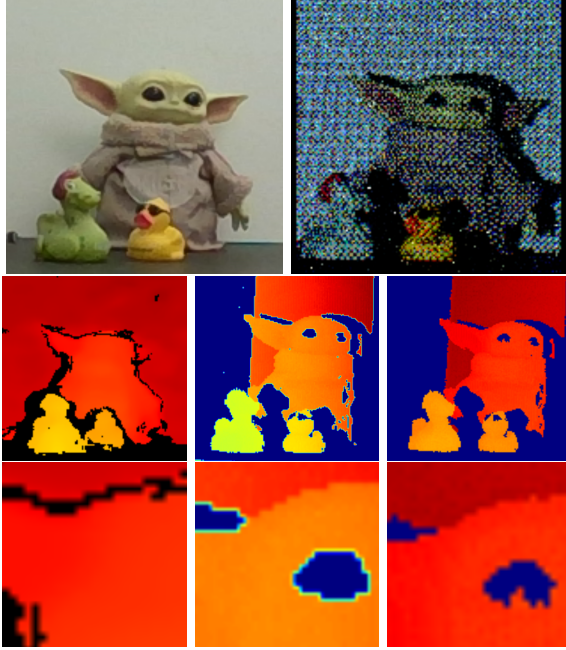
To reconstruct the color and depth, we introduced different pattern sequences, we will describe them separately in detail in the following subsections.

4.1 Color detection

As mentioned in Section 2 and shown in Figure 2, we project each pattern three times onto the scene with different wavelengths/colors, followed by capturing the reflection with the EC. These patterns could be part of a depth measuring procedure (moving line or dots) or a single pattern just to detect the color. Figure 4 shows the pattern sequence and their exposure times in microseconds. There are 4 different types of sequences to obtain color and/or depth. For instance, when measuring depth first and then color, any pattern from Figure 3 could be used to capture the color, even if the depth pattern is different. So, based on the needs, one pattern could be denser and have a higher CP than the other. One could use a solid pattern and decrease the Region of Interest (ROI) of the camera to prevent bus saturation while still obtaining a fully dense, colorful image for a specific area.

Since the projector and camera are connected through the external trigger pins, we projected a blank pattern with a specific exposure time as the ID, allowing the software to detect which pattern sequence mode is being projected by the projector. Both the ESL and X-maps methods utilize a Micro Electro-Mechanical System (MEMS) laser projector limited to 60 Hz, making them suitable for raster scanning patterns where rows are projected sequentially. In contrast, our work employs a Digital Micromirror Device (DMD projector) capable of projecting all pixels simultaneously, with a capacity exceeding 4 kHz. The top row of Figure 5 shows the RGB reconstructed by our method compared to the output color image of the RealSense D455 camera.

We evaluate the quality of our color reconstruction using a Macbeth ColorChecker chart, following standard color accuracy protocols, as established by Bayer (1976), Khashabi et al. (2014), and Ramanath et al. (2005). As shown in our previous work (Marjani-Bajestani and Beltrame (2023)), the method consistently reproduces color accurately, even though it uses only a monochrome event camera, supporting the effectiveness of the proposed active color projection approach.



D455: 33 ms ESL: 2.36 s ours: 12.57 ms

Fig. 5: Top Left: Output of the D455 RGB camera. **Top Right:** The RGB image reconstructed by the proposed method with a Monochrome EC. **Middle Row:** Depth detection comparison between D455 (Left), Muglikar et al. (2021)’s work named ESL (Middle), and our method, E-RGB-D (Right). **Bottom Row:** Zoomed-in view of the middle row. Note that the color differences are due to defining different minimum and maximum values for the jet-coded colorization; the actual difference in mm is detailed in Section 5.3.

4.2 Depth detection

Like X-maps, as proposed by Morgenstern et al. (2023), we provided a lookup table for disparity values to eliminate the need for disparity search. Because computing scene disparity by aligning time entries of the map along epipolar lines with an idealized projector time map is computationally intensive, as noted by Muglikar et al. (2021). However, our DMD projector does not exhibit raster printing behavior, so we did not store the projector’s x coordinates in relation to y and time t , and we do not use a temporal map either. Instead, we determine the disparity by knowing the column of the projected line. We will describe it in detail in this section.

Direct disparity lookup table: We formulate the problem of depth estimation using epipolar lines. After calibrating the system and setting up the stereo configuration, we create a lookup table LUT_c that assigns each pixel on the camera plane $P_c(x_c, y_c)$ to its corresponding pixel on the rectified camera’s image $P_{c_r}(x_{c_r}, y_{c_r})$. Additionally, a lookup table LUT_p assigns each pixel $P_p(x_p, y_p)$ on the projector plane to $P_{p_r}(x_{p_r}, y_{p_r})$ on the rectified projector image.

$$LUT_c(P_c(x_c, y_c)) = P_{c_r}(x_{c_r}, y_{c_r}) \quad (1)$$

$$LUT_p(P_p(x_p, y_p)) = P_{p_r}(x_{p_r}, y_{p_r}) \quad (2)$$

Considering that we are projecting different numbers of lines on the object, we could have an array *Columns* that carries the column number x_p of each line on the projector plane. As shown in Figure 4, the size of this lookup array could vary from 1 to n based on the pattern mode.

$$Columns = [x_{p_1} \ x_{p_2} \ \dots \ x_{p_n}] \quad (3)$$

By identifying which pattern is being projected and knowing the coordinates of the captured event, we can determine the disparity of the incoming event directly. Imagine at the time of receiving the $Event_c(x_c, y_c)$, we are projecting line number m ; then, we can determine two points of this line on the projector rectified map as:

$$Top_{p_r} = LUT_p(Columns[m], H) = (x_T, y_T) \quad (4)$$

$$Bottom_{p_r} = LUT_p(Columns[m], 0) = (x_B, y_B) \quad (5)$$

where H represents the height of the projector resolution.

Because our setup is a horizontal stereo, the epipolar lines in the rectified images are horizontal and have the same y -coordinate. The corresponding point is determined by calculating the intersection of the line that passes through these two points and the horizontal line that passes through the event’s pixel on the rectified camera plane.

$$Event_{c_r} = LUT_c(x_c, y_c) = (x_E, y_E) \quad (6)$$

$$x_{p_r} = x_T + (y_E - y_T) \cdot slope \quad (7)$$

where slope = $\frac{x_B - x_T}{y_B - y_T}$. And the disparity would be:

$$\text{disparity} = x_{p_r} - x_E \quad (8)$$

The depth Z of a point in a scene can be calculated using the formula:

$$Z = \frac{f \cdot B}{\text{disparity}} \quad (9)$$

where f is the focal length of the camera, B is the baseline. Algorithm 1 provides a concise overview of the entire process.

We were able to generate a temporal map similar to the ones produced by using raster printing projectors. Figure 6 displays the temporal map of Figure 5 setup, created by ESL and E-RGB-D (ours). Although we do not use the temporal map, this figure shows that we could generate one simply by knowing which column is being projected by the DMD projector and assigning a temporal index/color to that specific receiving event. However, in the other methods, they need to receive all events and normalize the temporal map based on the time of receiving the first and the last event.

Moreover, in X-maps, to obtain values for all possible measurements from the camera and create the lookup reference, they needed to record events at least for one time. However, we do not need to record anything and we can directly find out the depth by knowing the column of the projected line on the rectified projector image.

In practice, the projector’s resolution is usually higher than that of the camera sensor, which means the EC may not capture individual projector columns or may see overlapping columns. To address this, we introduced a gap between each line in our fully dense patterns, ensuring a solid, dense temporal map with the camera.

Our method publishes events, and a separate ROS node aggregates these events and publishes frames at various speeds. Since our system operates on an event-based model rather than a frame-based one, it does not require complete pattern captures. However, as a consequence of this approach, some patterns may not be fully captured at higher frequencies. This contrasts with traditional methods that rely on complete pattern captures to generate data. One metric for assessing output quality is the Fill Rate (FR), which compares the number of pixels containing data in the current frame to those in the ground truth frame. For instance, patterns with 23 lines

complete faster compared to those with 45 lines, allowing quicker coverage of the field of view and achieving a higher FR. However, reducing the number of lines sacrifices detail. This trade-off between speed and detail is a deliberate aspect of our approach, which is not achievable with other methods. Raster-based projectors frequently project a solid pattern, while methods using coded patterns like grayscale or binary codes require capturing all patterns to report depth. They cannot increase speed by reducing detail, nor can they enhance detail by sacrificing speed.

Algorithm 1 Stamping events with depth and color

- 1: Initialize LUT_p , LUT_c , and $Columns$ based on calibration and pattern mode
 - 2: **while** camera triggers events **do**
 - 3: **if** external trigger **then**
 - 4: Increment m and/or indicate the new color
 - 5: **else**
 - 6: Capture $Event_c(x_c, y_c)$
 - 7: Retrieve $Event_{c_r}(x_E, y_E)$ from $LUT_c(x_c, y_c)$
 - 8: Retrieve x_p from $Columns[m]$
 - 9: Retrieve $Top_{p_r}(x_T, y_T)$ and $Bottom_{p_r}(x_B, y_B)$ from $LUT_p(x_p, H)$ and $LUT_p(x_p, 0)$
 - 10: Calculate $x_{p_r} = x_T + (y_E - y_T) \cdot \frac{x_B - x_T}{y_B - y_T}$
 - 11: Compute depth = $\frac{f \cdot B}{x_{p_r} - x_E}$
 - 12: Publish depth and color-stamped events alongside the colored point cloud on ROS topics.
 - 13: **end if**
 - 14: **end while**
-

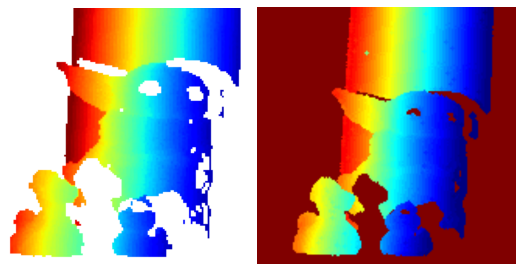


Fig. 6: Temporal map reconstructed by ESL (Left), ours E-RGB-D (Right).

5 Experiments

This section assesses the performance of our event-based SL system for depth and color estimation. We begin by introducing the hardware setup (Section 5.1), along with the baseline methods and ground truth used for comparison (Section 5.2). Subsequently, we conduct experiments on static scenes to quantify the accuracy of the proposed method and on dynamic scenes to demonstrate its high-speed acquisition capabilities (Section 5.3).

5.1 Setup

Camera: The event camera used in this study is the Prophesee Evaluation Kit 1 (EVK1) equipped with a Gen 3.0 sensor (Prophesee (2024)). This dynamic vision sensor offers a resolution of 640×480 pixels with a $15 \mu\text{m}$ pixel pitch and only detects contrast changes. It features a dynamic range greater than 120 dB, an average latency of $200 \mu\text{s}$, and timestamps events with microsecond precision (Figure 8).

Projector: To project binary patterns at high speed (over 4 kHz), we used the Texas Instruments (2024) DLP LightCrafter 4500 projector, which supports a resolution of 912×1140 in a diamond pixel configuration and operates with a $235 \mu\text{s}$ exposure period, allowing a 4.225 kHz pattern-switching rate that is easily captured by the EC (Figure 8). Because of the diamond pixel array of the DMD, the pixel data does not appear on the DMD exactly as it would in an orthogonal pixel arrangement. Figure 7 shows the pattern that we used to project dots in our dot-based patterns.

Calibration: To calibrate the system, we introduced a camera-projector calibration procedure specifically designed for event-based SL. Our method involves calibrating the intrinsic parameters of the event camera by utilizing a standard calibration tool (OpenCV; Bradski (2000)) applied to images obtained by converting events into intensity frames. This conversion is done while observing a flickering circle-grid pattern from various angles. We chose circle patterns over checkerboards due to their superior performance in terms of both the quality and stability of the final calibration results across multiple iterations, as shown by Kaehler and Bradski (2017). Unlike checkerboards, which may lead to uncertainties in corner detection, circle-grid patterns

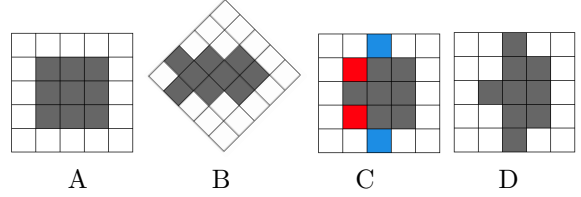


Fig. 7: The pattern of one dot with the size of 3×3 pixels in our dot-based patterns. If we project (A) due to the diamond pixel configuration of the DMD, we will see (B) on the object surface. Which could lead to mislocating the center of the projected dot. Therefore, we should move red-colored pixels to blue ones in (C) and project (D) to achieve the pattern (A) on the object’s surface with a 45-degree rotation.

allow for more precise extraction of circle centers, for instance, through the calculation of the center of gravity of all circle pixels.

Our approach for this calibration is straightforward and adaptable. We begin by setting up a circle grid of flickering LEDs on a flat surface and projecting another circle grid pattern using the projector beside it on the board. After calibrating the intrinsic parameters of the event camera using the LED circle-grid pattern, we proceed to calibrate the extrinsic parameters of the camera-projector setup and the intrinsic parameters of the projector.

Once the camera calibration is complete, we determine the board’s relative position, which in turn allows us to calibrate the projector. This streamlined method enables the simultaneous calibration of all parameters through simple operations, significantly reducing the complexity typically associated with calibration processes. Furthermore, it is universally applicable to all event-based SL systems. Figure 8 shows the calibration circle dot-board used for calibrating the system.

Luo et al. (2014) proposed an alternative approach for calibrating the SL camera-projector system. Their method involves introducing four reference planes and generating lookup tables for pixel correspondences. While this method can enhance calibration quality, it adds complexity to the procedure.

Similarly, Wang et al. (2020) presented a calibration technique based on Temporal Matrices Mapping (TMM). They utilized two temporal matrices to establish pixel correspondences between the SL projector plane and the event camera (EC) plane. Although this approach can improve calibration accuracy, it also increases the overall complexity of the calibration process.

Software: We have implemented our method on the Robot Operating System (ROS). The designed Qt-based Graphical User Interface (GUI) enables us to control the camera settings online and allows the ROS nodes to publish color- and depth-stamped events alongside RGB frames and colorful point clouds on ROS topics, as shown by Marjani-Bajestani and Beltrame (2025). More details can be found on our Event-based RGBD ROS Wrapper (see Marjani-Bajestani and Beltrame (2023)) Git repository at github.com/MISTLab/event_based_rgbd_ros.

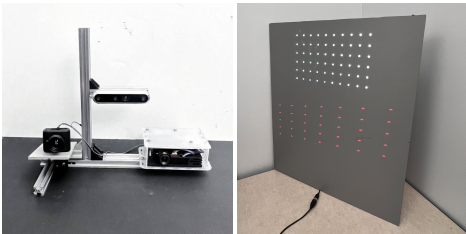


Fig. 8: Left: The experimental setup includes a DLP LightCrafter 4500 Evaluation Module, a Prophesee evaluation kit (Gen3-VGA), and an Intel RealSense D455 (only used for comparison). **Right:** The calibration circle dot-board used for calibrating the EC and camera-projector setup, with white dots from LEDs and red dots projected by the projector.

5.2 Baseline and Ground Truth

As shown in Table 1, the most recent related works are the ESL, as proposed by Muglikar et al. (2021), the X-maps, as introduced by Morgenstern et al. (2023), and the SEG, as described by Lu et al. (2024). Since all of them used a laser point projector with a scanning speed of 60 Hz, they were automatically excluded from comparison in high-speed real-time event-based scanning.

Although X-maps presents a high-speed structured light method using event cameras, it relies on a raster-scanning laser projector and constructs a rectified X-map from a time-discretized spatio-temporal event cuboid. Our system, in contrast, does not accumulate or discretize events into frames; it instead performs disparity estimation and 3D reconstruction per event in real-time. Due to these fundamental differences in both hardware and methodology, direct benchmarking with X-maps is not feasible. Therefore, we focused our comparisons on ESL, as proposed by Muglikar et al. (2021), which is compatible with recorded data and serves as a fair, reproducible baseline for evaluating our method in a similar structured light context.

Since, the ESL used a raw recorded event file and pre-data-processing to synchronize and convert the raw event data file in the absence of triggers. This makes it more accurate (but slower) than the X-maps method because it considers all events together rather than processing them in real-time. More importantly, we could still generate the time-maps even by using a DLP. We did not use the SEG method in dynamic conditions because their code is not yet publicly available.

In this task, obtaining the GT is challenging due to the lack of methods capable of producing dense depth with accuracy above the millimeter level for natural scenes. Therefore, ESL, as proposed by Muglikar et al. (2021), adopts averaged MC3D, as introduced by Matsuda et al. (2015), as their ground truth, whereas X-maps, as described by Morgenstern et al. (2023), employ optimized ESL. While we acknowledge the potential for accuracy enhancement through averaging operations in depth estimation, our approach differs due to reconstructing color alongside depth. Given the utilization of a distinct point scanning method and projector type, we developed our method to generate the ground truth by accumulating more events over an extended time window (one second) and performing averaging across 10 scans.

5.3 Results

Static Environments: To evaluate the outcome of the proposed method in static situations, we have designed seven different setups (see Figure 10). We utilized line and dot patterns in modes 3 and 4 (see Figure 3). It is necessary to

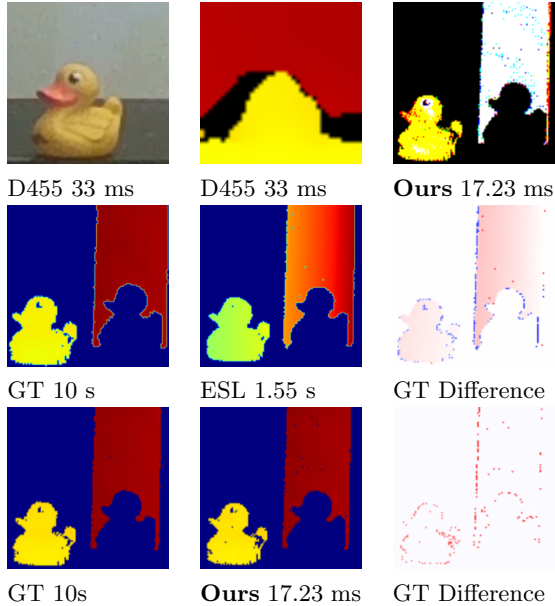


Fig. 9: Comparison of color and depth detection for Duck setup (M4L23 pattern).

mention that in mode 4, the color and depth patterns are the same. However, in mode 3, different patterns can be used (e.g., in mode 3, we utilized dot/line patterns to detect depth but used dot patterns to detect color). To provide abbreviated names for each pattern sequence, we used the following method: for example, 'M3L45' indicates mode 3 with 45 lines in the pattern for depth detection.

Projecting 23 patterns, along with color patterns, in mode 3 takes 7.4 ms, while projecting 23 patterns three times in mode 4 takes 17.23 ms. Projecting 45 patterns along with the color patterns in mode 3 takes 12.57 ms. To scan static objects, we used the patterns M3L45, M3D45, and M4L23.

Each pattern falls into one of three categories: wide, normal, and dense. To indicate the category, we used Coverage Percentage (CP). To calculate the CP, we consider the area size between the first and last lines rather than the entire projector plane. Otherwise, considering 45 lines dense or sparse would yield the same CP. In general, a higher CP in our case indicates a denser pattern with a smaller field of view (FOV), while a lower CP suggests a more sparse pattern that covers a larger area with a higher FOV.

Our evaluation spanned three different speeds: 1, 26, and 58 fps. However, as mentioned in Subsection 4.2, our system is an event-based model rather than a frame-based one.

Detailed statistical analyses (e.g., Analysis of Variance (ANOVA) tables and raincloud figures) supporting these results are provided in the supplementary materials. For additional evaluation of color accuracy, including a Macbeth ColorChecker benchmark, we refer readers to our earlier work (see Marjani-Bajestani and Beltrame (2023)).

Figure 9 illustrates color and depth detection for the Duck setup using pattern M4L23. Our method achieves depth frame reconstruction about 90 times faster than the ESL method, while also simultaneously reconstructing color. Compared to RealSense, our method provides sharper and more accurate results. For a comprehensive comparison of all setups in a static scenario, refer to Figure 10.

Dynamic Environments: To evaluate the outcome of the proposed method in dynamic situations, we have designed five different setups. To scan dynamic objects, we used the patterns M3D45, M3L23, and M3D23. We did not utilize pattern M4L23, although it has better output in terms of color in low-speed scanning. This is because considering the number of patterns that it needs to project, the total scanning speed could decrease, which is critical in dynamic conditions.

Since there is no GT as mentioned in Subsection 5.2, we could not provide FR or RMSE for dynamic experiments. Figure 11 shows the color and depth detection of a volleyball ball being thrown up in front of the setup at a distance of approximately 1.5 m, using pattern M3L23. It also shows that the D455 sensor captured a slightly blurred RGB image, and the depth detection is not sharp and accurate.

6 Conclusion

This study introduces a method for generating colored point clouds with adjustable speed and resolution, enabling depth map creation in challenging environments like dynamic and low-light conditions, even with stationary cameras or objects.

Results show that denser scanning patterns provide more accurate data for smaller fields of view (FOV), while sparser patterns cover larger

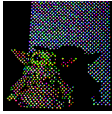
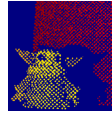
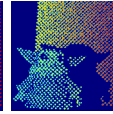
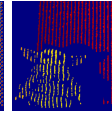
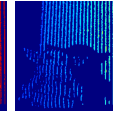
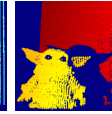
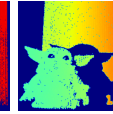
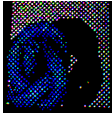
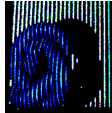
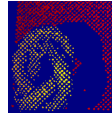
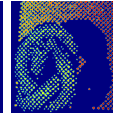
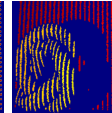
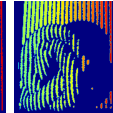
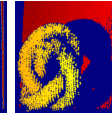
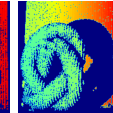
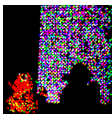
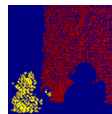
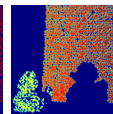
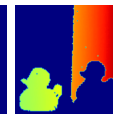
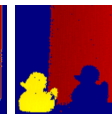
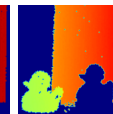
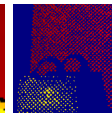
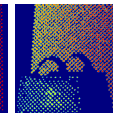
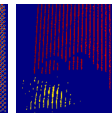
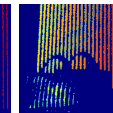
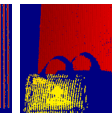
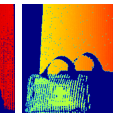
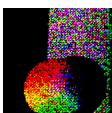
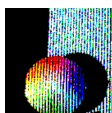
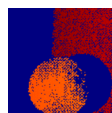
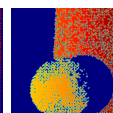
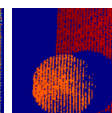
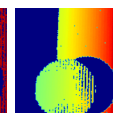
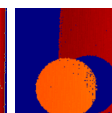
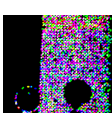
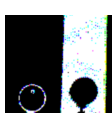
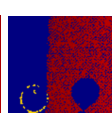
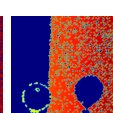
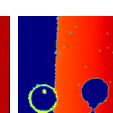
	D455	Ours	Ours	D455	Ours	ESL	Ours	ESL	Ours	ESL
	33.33 ms	M3D45	M4L23	33.33 ms	M3D45	M3D45	M4L23	M4L23	M3L45	M3L45
	RGB	RGB	RGB	Depth	Depth	Depth	Depth	Depth	Depth	Depth
Yoda										
	RMSE:	20.04	22.42		330.23	300.84	228.03	241.12	335.03	199.83
	Time:	12.57 ms	17.23 ms		12.57 ms	2.35 s	17.23 ms	1.93 s	12.57 ms	5.37 s
Foam										
	RMSE:	19.11	17.51		328.98	334.30	198.69	196.33	161.86	213.26
	Time:	12.57 ms	17.23 ms		12.57 ms	1.97 s	17.23 ms	2.70 s	12.57 ms	4.33 s
Duck										
	RMSE:	18.64	12.48		189.59	238.92	77.56	74.10	85.28	87.03
	Time:	12.57 ms	17.23 ms		12.57 ms	2.35 s	17.23 ms	1.55 s	12.57 ms	5.37 s
Bag										
	RMSE:	22.38	21.53		371.73	385.64	222.13	189.69	326.28	153.63
	Time:	12.57 ms	17.23 ms		12.57 ms	2.33 s	17.23 ms	2.14 s	12.57 ms	4.71 s
Circle										
	RMSE:	19.03	18.43		166.77	111.57	199.34	170.33	83.11	74.41
	Time:	12.57 ms	17.23 ms		12.57 ms	1.98 s	17.23 ms	2.59 s	12.57 ms	2.62 s
Stand										
	RMSE:	20.46	12.53		181.56	121.65	83.32	100.22	85.25	71.84
	Time:	12.57 ms	17.23 ms		12.57 ms	2.19 s	17.23 ms	1.60 s	12.57 ms	2.79 s

Fig. 10: Comparison of color and depth detection for static scenes between RealSense D455, ESL, and E-RGB-D (ours). Noting that the available code for ESL needs to create a temporal map as a numpy array from a recorded raw file, we did not include the time required for these processes in our calculations. We only considered the time needed for calculating depth from those files. The operating system had an NVIDIA(R) GeForce RTX(TM) 2060 6GB GPU and an Intel Core i7-9750H CPU with 16GB of memory.

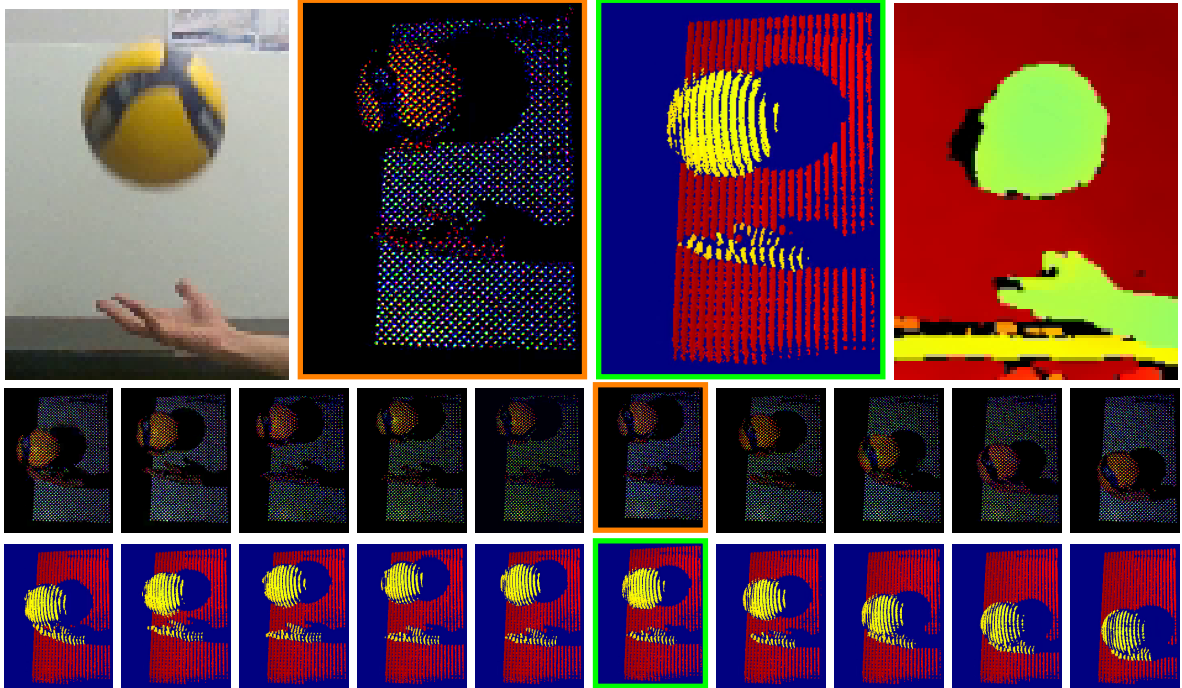


Fig. 11: Comparison of color and depth detection for dynamic scenes (setup with ball number one) between RealSense D455 (top row, right and left) and our system (middle, using pattern M3L23).

areas. Using fewer patterns, we achieved a scanning time of 7.4 ms, significantly faster than the RealSense D455 (33 ms) and the ESL method (2 to 5 seconds). This method balances detail and speed effectively, offering improved speed control and enabling color reconstruction.

Using this setup, we achieved color scanning speeds up to 1.4 kHz (Mode 1, as investigated in our previous work) and pixel-based depth scanning speeds up to 4 kHz (Mode 2 with $n = 1$). This provides a continuous stream of annotated events with color and depth, along with detailed, colorful point cloud output. The method shows versatility across static and dynamic environments, introducing an innovative strategy for balancing resolution and acquisition speed.

Compared to prior methods that rely on frame accumulation or raster scanning, our approach offers a truly asynchronous pipeline with real-time event tagging. This allows color and depth sensing to occur independently of scene complexity or temporal batching, making it highly suitable for applications requiring low latency, high responsiveness, and continuous high-speed acquisition. This architectural advantage becomes especially

critical in dynamic or resource-constrained environments.

An important feature of our system is its flexibility in structured light pattern design. While we demonstrate several effective patterns in this work, the system is capable of supporting custom encodings as long as they can be projected by the DLP hardware. Our software architecture is designed to accommodate such variations seamlessly, making the proposed method scalable and adaptable for a range of use cases, from mobile robotics to industrial metrology.

In light of the findings and outcomes of this study, several promising avenues for future research have emerged:

1. **Optimizing resolution of color and depth detection** by projecting a denser pattern in a specific area could be achieved through the implementation of a movement detection algorithm during SL light downtime or by using a secondary camera to detect movement in parallel.
2. **Increasing scanning speed** at the cost of higher bandwidth usage, while reducing resolution, can be achieved by projecting

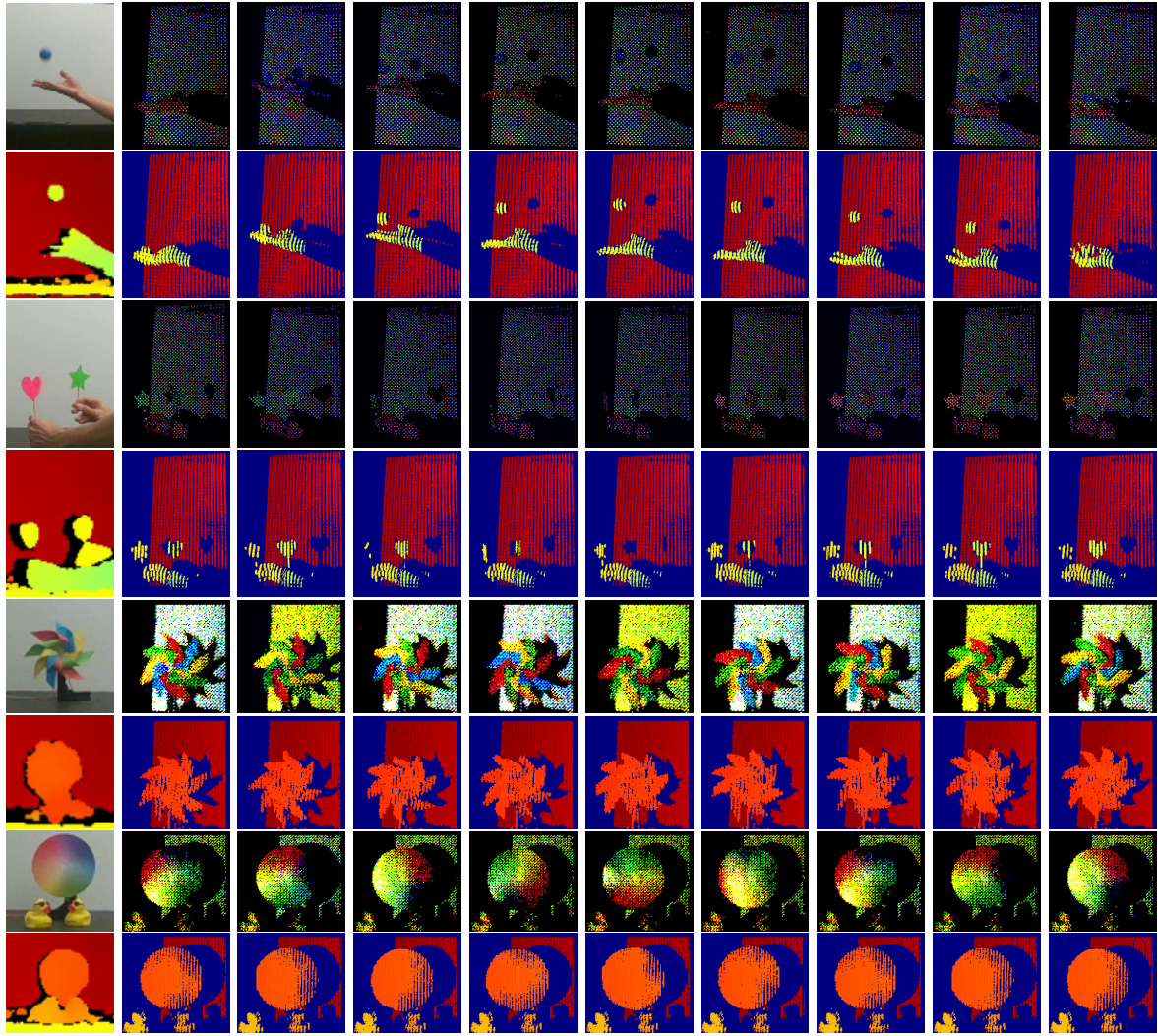


Fig. 12: Series of images showing color and depth detection for dynamic scenes, scanned in 7.4 to 17.23 ms using the M3L23 pattern. The images in the first column from the left were captured by the RealSense D455 for comparison, which took 33 ms.

white-colored patterns when utilizing a color event camera (EC).

3. **Optimizing depth measurement** based on the SL wavelength and the object's surface color by controlling the current of each LED of the projector.
4. **Increasing the scanning range** by utilizing a Near-IR projector instead of capturing color.

5. **Investigating predictive techniques** such as neighboring pixel tracking or learning-based interpolation to enhance the completeness of reconstructed color frames in regions with sparse event activity.

Supplementary information. Detailed statistical analyses supporting these findings, including Analysis of Variance (ANOVA) tables and raincloud figures, are presented in the supplementary materials, as mentioned in Subsection 5.3. For further assessment of color accuracy, such as

evaluations using a Macbeth ColorChecker benchmark, readers are directed to our previous study (Marjani-Bajestani and Beltrame (2023)).

Acknowledgements. This paper was produced by MIST Lab. thanks to the NSERC Discovery Grant 2019-05165, at the Department of Computer Engineering and Software Engineering, Polytechnique Montreal, Montreal, CA.

References

- Allen M, Poggiali D, Whitaker K, Marshall TR, van Langen J, Kievit RA. Raincloud plots: a multi-platform tool for robust data visualization. Wellcome open research. 2019;4. <https://doi.org/10.12688/wellcomeopenres.15191.2>.
- Bayer BE. Color imaging array. United States Patent 3,971,065. 1976;.
- Bradski G. The OpenCV Library. Dr Dobb's Journal of Software Tools. 2000;<https://github.com/opencv>.
- Brandli C, Mantel T, Hutter M, Höpfinger M, Berner R, Siegwart R, et al. Adaptive pulsed laser line extraction for terrain reconstruction using a dynamic vision sensor. *Frontiers in neuroscience*. 2014;7:275. <https://doi.org/10.3389/fnins.2013.00275>.
- Cohen Duwek H, Ezra Tsur E. Colorful image reconstruction from neuromorphic event cameras with biologically inspired deep color fusion neural networks. *Bioinspiration & Biomimetics*. 2024 mar;19(3):036001. <https://doi.org/10.1088/1748-3190/ad2a7c>.
- Geng J. DLP-based structured light 3D imaging technologies and applications. In: Douglass MR, Oden PI, editors. *Emerging Digital Micromirror Device Based Systems and Applications III*, vol. 7932 International Society for Optics and Photonics, SPIE; 2011. p. 79320B. <https://doi.org/10.1117/12.873125>.
- Gupta M, Nayar SK. Micro phase shifting. In: 2012 IEEE Conference on Computer Vision and Pattern Recognition IEEE; 2012. p. 813–820. <https://doi.org/10.1109/CVPR.2012.6247753>.
- Gupta M, Yin Q, Nayar SK. Structured light in sunlight. In: 2013 IEEE International Conference on Computer Vision (ICCV); 2013. p. 545–552. <https://doi.org/10.1109/ICCV.2013.73>.
- Huang X, Zhang Y, Xiong Z. High-speed structured light based 3D scanning using an event camera. *Optics Express*. 2021;29(22):35864–35876. <https://doi.org/10.1364/OE.437944>.
- Intel RealSense.: Stereo depth solutions; 2025. <https://realsenseai.com/>, accessed: 2025-11-23.
- Jang HW, Jung YJ. Deep Color Transfer for Color-Plus-Mono Dual Cameras. *Sensors*. 2020;20(9):2743. <https://doi.org/10.3390/s20092743>.
- JASP Team.: JASP (Version 0.18.3); 2024. <https://jasp-stats.org/>. Computer software.
- Kaehler A, Bradski G. Learning OpenCV 3. O'Reilly Media; 2017. <https://www.oreilly.com/library/view/learning-opencv-3/9781491937983/>, iSBN-10: 1491937998.
- Khashabi D, Nowozin S, Jancsary J, Fitzgibbon AW. Joint Demosaicing and Denoising via Learned Nonparametric Random Fields. *IEEE Transactions on Image Processing*. 2014;23(12):4968–4981. <https://doi.org/10.1109/TIP.2014.2359774>.
- Leroux T, Ieng SH, Benosman R. Event-based structured light for depth reconstruction using frequency tagged light patterns. arXiv preprint arXiv:1811.10771. 2018;<https://doi.org/10.48550/arXiv.1811.10771>.
- Levin A, Lischinski D, Weiss Y. Colorization using optimization. In: ACM SIGGRAPH 2004 Papers; 2004. p. 689–694. <https://doi.org/10.1145/1186562.1015780>.
- Li C, Brandli C, Berner R, Liu H, Yang M, Liu SC, et al. Design of an RGBW color VGA rolling and global shutter dynamic and active-pixel vision sensor. In: 2015 IEEE International Symposium on Circuits and Systems (ISCAS) IEEE; 2015. p. 718–721. <https://doi.org/10.1109/ISCAS.2015.7168734>.

- Li Y, Jiang H, Xu C, Liu L. Event-driven Fringe Projection Structured Light 3D Reconstruction based on Time-frequency Analysis. *IEEE Sensors Journal*. 2024;<https://doi.org/10.1109/JSEN.2024.3349432>.
- Li Y, Xu C, Liu L. Learning from General Diffuse Surfaces: An Event-driven Approach for High Dynamic Range Industrial Optical Measurement. *Optics & Laser Technology*. 2024;177:111183. <https://doi.org/10.1016/j.optlastec.2024.111183>.
- Lu X, Sun L, Gu D, Xu Z, Wang K. SGE: Structured Light System Based on Gray Code with an Event Camera. arXiv preprint arXiv:240307326. 2024;<https://doi.org/10.48550/arXiv.2403.07326>.
- LUCID Vision Labs.: Helios Time-of-Flight (ToF) Camera; 2025. <https://thinklucid.com/helios-time-of-flight-tof-camera/>, accessed: 2025-11-24.
- Luo H, Xu J, Binh NH, Liu S, Zhang C, Chen K. A simple calibration procedure for structured light system. *Optics and Lasers in Engineering*. 2014;57:6–12. <http://doi.org/10.1016/j.optlaseng.2014.01.010>.
- Mangalore AR, Seelamantula CS, Thakur CS. Neuromorphic Fringe Projection Profilometry. *IEEE Signal Processing Letters*. 2020;27:1510–1514. <https://doi.org/10.1109/LSP.2020.3016251>.
- Marcireau A, Ieng SH, Simon-Chane C, Benosman RB. Event-Based Color Segmentation With a High Dynamic Range Sensor. *Frontiers in neuroscience*. 2018;12:135. <https://doi.org/10.3389/fnins.2018.00135>.
- Marjani-Bajestani SE, Beltrame G. Event-Based RGB Sensing With Structured Light. In: *Proceedings of the IEEE/CVF Winter Conference on Applications of Computer Vision (WACV)*; 2023. p. 5458–5467. <https://doi.org/10.1109/WACV56688.2023.00542>.
- Marjani-Bajestani SE, Beltrame G. Event-Based Vision for Robot Soccer. In: Barros E, Hanna JP, Okada H, Torta E, editors. *RoboCup 2024: Robot World Cup XXVII Cham*: Springer Nature Switzerland; 2025. p. 309–317. https://doi.org/10.1007/978-3-031-85859-8_26.
- Marrugo AG, Gao F, Zhang S. State-of-the-art active optical techniques for three-dimensional surface metrology: a review. *J Opt Soc Am A (JOSA A)*. 2020;37(9):B60–B77. <http://doi.org/10.1364/JOSAA.398644>.
- Martel JN, Müller J, Conradt J, Sandamirskaya Y. An Active Approach to Solving the Stereo Matching Problem using Event-Based Sensors. In: *2018 IEEE International Symposium on Circuits and Systems (ISCAS)* IEEE; 2018. p. 1–5. <https://doi.org/10.1109/ISCAS.2018.8351411>.
- Matsuda N, Cossairt O, Gupta M. MC3D: Motion Contrast 3D Scanning. In: *2015 IEEE International Conference on Computational Photography (ICCP)* IEEE, IEEE; 2015. p. 1–10. <https://doi.org/10.1109/ICCPHOT.2015.7168370>.
- Microsoft Kinect.: Microsoft Kinect for Xbox 360; 2010. <https://www.microsoft.com/en-us/download/details.aspx?id=40278>, accessed: 2025-12-01.
- Moeys DP, Corradi F, Li C, Bamford SA, Longinotti L, Voigt FF, et al. A Sensitive Dynamic and Active Pixel Vision Sensor for Color or Neural Imaging Applications. *IEEE transactions on biomedical circuits and systems*. 2017;12(1):123–136. <https://doi.org/10.1109/TBCAS.2017.2759783>.
- Moeys DP, Li C, Martel JN, Bamford S, Longinotti L, Motsnyi V, et al. Color temporal contrast sensitivity in dynamic vision sensors. In: *2017 IEEE International Symposium on Circuits and Systems (ISCAS)* IEEE; 2017. p. 1–4. <https://doi.org/10.1109/ISCAS.2017.8050412>.
- Morar A, Moldoveanu A, Mocanu I, Moldoveanu F, Radoi IE, Asavei V, et al. A Comprehensive Survey of Indoor Localization Methods Based on Computer Vision. *Sensors*. 2020;20(9):2641. <https://doi.org/10.3390/s20092641>.
- Morgenstern W, Gard N, Baumann S, Hilsman A, Eisert P. X-maps: Direct Depth

- Lookup for Event-based Structured Light Systems. In: 2023 IEEE/CVF Conference on Computer Vision and Pattern Recognition Workshops (CVPRW); 2023. p. 4006–4014. <https://doi.org/10.1109/CVPRW59228.2023.00418>.
- Muglikar M, Gallego G, Scaramuzza D. ESL: Event-based Structured Light. In: 2021 International Conference on 3D Vision (3DV) IEEE; 2021. p. 1165–1174. <https://doi.org/10.1109/3DV53792.2021.00124>.
- Orbbec, Astra Series.: Intelligent computing for everyone, everywhere; 2025. <https://www.orbbec.com/products/structured-light-camera/astra-2/>, accessed: 2025-11-23.
- Prophesee.: Evaluation Kit; 2024. <https://www.prophesee.ai/event-based-evk/>, accessed: 2025-01-15.
- Ramanath R, Snyder WE, Yoo Y, Drew MS. Color image processing pipeline. IEEE Signal Processing Magazine. 2005;22(1):34–43. <https://doi.org/10.1109/MSP.2005.1407713>.
- Texas Instruments.: Digital Light Processing LightCrafter 4500; 2024. <https://www.ti.com/tool/DLPLCR4500EVM>, accessed: 2025-01-15.
- Tin SK, Ye J, Nezamabadi M, Chen C. 3D reconstruction of mirror-type objects using efficient ray coding. In: 2016 IEEE International Conference on Computational Photography (ICCP) IEEE; 2016. p. 1–11. <https://doi.org/10.1109/ICCPHOT.2016.7492867>.
- Trémeau A, Tominaga S, Plataniotis K. Color in image and video processing: most recent trends and future research directions. EURASIP Journal on Image and Video Processing. 2008;2008:1–26. <https://doi.org/10.1155/2008/581371>.
- Wang G, Feng C, Hu X, Yang H. Temporal Matrices Mapping Based Calibration Method for Event-Driven Structured Light Systems. IEEE Sensors Journal. 2020;<https://doi.org/10.1109/JSEN.2020.3016833>.
- Wang H, Liu T, He C, Li C, Liu J, Yu L. Enhancing Event-based Structured Light Imaging with a Single Frame. In: 2022 IEEE International Conference on Multisensor Fusion and Integration for Intelligent Systems (MFI) IEEE; 2022. p. 1–7. <https://doi.org/10.1109/MFI55806.2022.9913845>.
- Weikersdorfer D, Adrian DB, Cremers D, Conradt J. Event-based 3D SLAM with a depth-augmented dynamic vision sensor. In: 2014 IEEE International Conference on Robotics and Automation (ICRA) IEEE; 2014. p. 359–364. <https://doi.org/10.1109/ICRA.2014.6906882>.
- Willomitzer F, Häusler G. Single-shot 3D motion picture camera with a dense point cloud. Optics express. 2017;25(19):23451–23464. <http://doi.org/10.1364/OE.25.023451>.
- Wu K, Tan J, Xia H, Liu C. An exposure fusion-based structured light approach for the 3D measurement of a specular surface. IEEE Sensors Journal. 2020;<https://doi.org/10.1109/JSEN.2020.3027317>.
- Yu J, Gao N, Zhang Z, Meng Z. High Sensitivity Fringe Projection Profilometry Combining Optimal Fringe Frequency and Optimal Fringe Direction. Optics and Lasers in Engineering. 2020;129:106068. <http://doi.org/10.1016/j.optlaseng.2020.106068>.
- Zhang R, Isola P, Efros AA. Colorful Image Colorization. In: European conference on computer vision Springer; 2016. p. 649–666. https://link.springer.com/chapter/10.1007/978-3-319-46487-9_40.
- Zhao Z, Gu F, Xie P, Cao H, Song Z. Miniature 3D Depth Camera for Real-time Reconstruction. In: 2019 IEEE International Conference on Robotics and Biomimetics (ROBIO) IEEE; 2019. p. 1769–1776. <https://doi.org/10.1109/ROBIO49542.2019.8961795>.

A Supplementary Materials

Figures 13 and 14 are raincloud plots Allen et al. (2019) of accuracy metrics for color detection (PSNR, RMSE, FR) over more than 25k frames of data.

Analysis of Variance (ANOVA) (Tables 2 to 6) shows significant effects of both the Speed and CP factors (as well as their interaction) on the dependent variables (PSNR, RMSE, and FR). Residuals meet the normality assumption, supported by Q-Q plots in Figures 15 and 16, validating the model. These results confirm the statistical validity of our work. ANOVA tables were generated using JASP JASP Team (2024).

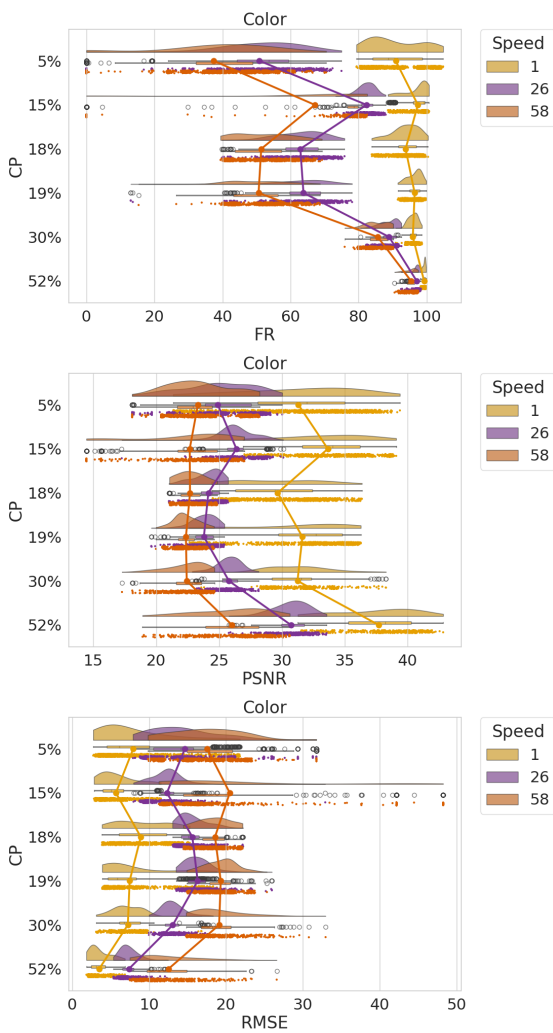


Fig. 13: Comparison of color detection for all setups at different speeds.

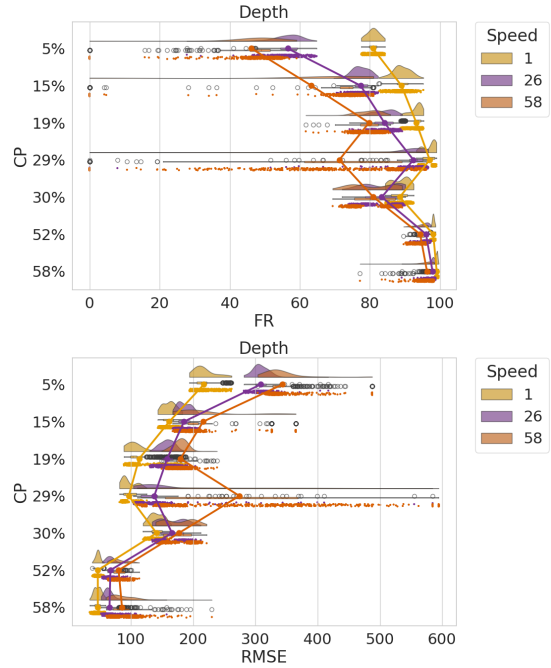


Fig. 14: Comparison of depth detection for all setups at different speeds.

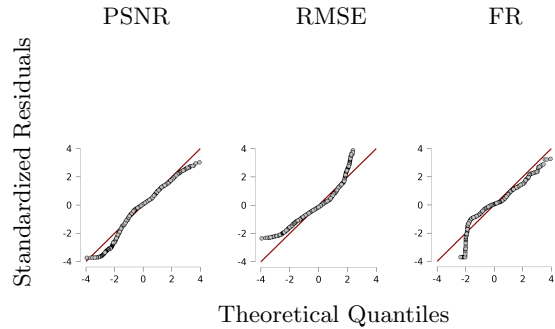


Fig. 15: Quantile-Quantile plots of the color detection dataset.

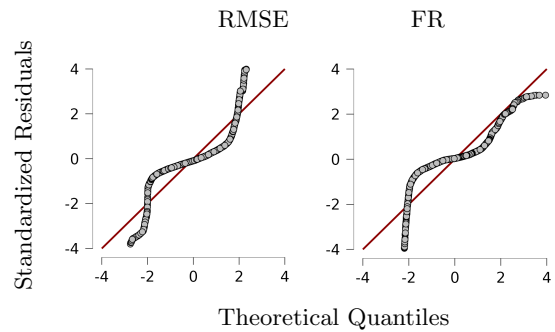


Fig. 16: Quantile-Quantile plots of the depth detection dataset.

Table 2: Analysis of Variance (ANOVA) for the Color PSNR

Cases	Sum of Squares	df	Mean Square	F	p
Speed	164027.653	2	82013.826	11569.337	< .001
CP	33584.097	5	6716.819	947.513	< .001
Speed * CP	6169.135	10	616.913	87.025	< .001
Residuals	89192.490	12582	7.089		

Table 3: Analysis of Variance (ANOVA) for the Color RMSE

Cases	Sum of Squares	df	Mean Square	F	p
Speed	225230.139	2	112615.070	7267.745	< .001
CP	42003.544	5	8400.709	542.150	< .001
Speed * CP	12562.719	10	1256.272	81.075	< .001
Residuals	194960.457	12582	15.495		

Table 4: Analysis of Variance (ANOVA) for the Color FR

Cases	Sum of Squares	df	Mean Square	F	p
Speed	$1.814 \times 10^{+6}$	2	906934.152	8884.279	< .001
CP	$1.897 \times 10^{+6}$	5	379446.459	3717.037	< .001
Speed * CP	658311.623	10	65831.162	644.879	< .001
Residuals	$1.284 \times 10^{+6}$	12582	102.083		

Table 5: Analysis of Variance (ANOVA) for the Depth RMSE

Cases	Sum of Squares	df	Mean Square	F	p
Speed	$1.136 \times 10^{+7}$	2	$5.680 \times 10^{+6}$	4288.971	< .001
CP	$6.380 \times 10^{+7}$	6	$1.063 \times 10^{+7}$	8028.498	< .001
Speed * CP	$6.595 \times 10^{+6}$	12	549596.715	414.970	< .001
Residuals	$1.666 \times 10^{+7}$	12579	1324.425		

Table 6: Analysis of Variance (ANOVA) for the Depth FR

Cases	Sum of Squares	df	Mean Square	F	p
Speed	518315.917	2	259157.958	3401.744	< .001
CP	$1.689 \times 10^{+6}$	6	281427.178	3694.053	< .001
Speed * CP	329420.234	12	27451.686	360.335	< .001
Residuals	958316.716	12579	76.184		